LANGMUIR

pubs.acs.org/Langmuir

Article

Nanosheet Synthesis of Mixed Co_3O_4/CuO *via* Combustion Method for Methanol Oxidation and Carbon Dioxide Reduction

Roshan Nazir,* Alanoud Khalfani, Omnia Abdelfattah, Anand Kumar, Mohammed Ali Saleh Saad, and Sardar Ali

Cite This: *Langmuir* 2020, 36, 12760−12771

ABSTRACT: This paper represents a study of mixed Co_3O_4/CuO nanosheet (NS) synthesis *via* solution combustion synthesis for oxidation of methanol and carbon dioxide (CO_2) conversion. The mixed oxide NS of Co_3O_4/CuO is a hybrid structure of Co_3O_4 and CuO NSs. We applied this mixed oxide NS of Co_3O_4/CuO for methanol oxidation and carbon dioxide (CO_2) conversion, and the results revealed that the activity of the mixed oxide NS surpassed the activity of the corresponding individual Co_3O_4 and CuO metal oxide NSs, both in methanol oxidation and in CO_2 conversion. The mass activity of the mixed Co_3O_4/CuO NS produced at 0.627 V versus Ag/AgCl during methanol oxidation (0.5 M) was 12 mA g^{-1}, which is 2.4 times better than that of Co_3O_4, whose mass activity is 5 mA g^{-1}, and 4 times better than that of the CuO NS, whose mass activity is 3 mA g^{-1}. The methanol oxidation peak at 0.62 V versus Ag/AgCl was also more intense than individual oxides. The trend in performance of methanol oxidation follows the order: Co_3O_4/CuO > Co_3O_4 > CuO. In the case of CO_2 reduction, we experienced that our product was formate, and this was proved by formate oxidation (formate is formed as a product during the reduction of CO_2) on the surface of the Pt ring of a rotating ring-disc electrode. Similar to methanol oxidation, Co_3O_4/CuO also showed superior activity in carbon dioxide reduction. It was experienced that at −1.5 V, the current density rises to −24 mA/cm^2 for the Co_3O_4/CuO NS, that is, 0.6 times that of the CuO NS, which is −15 mA/cm^2, and 3 times more than that of the Co_3O_4 NS, which is 8 mA/cm^2. The trend in performance of CO_2 reduction follows the order: Co_3O_4/CuO > CuO > Co_3O_4.

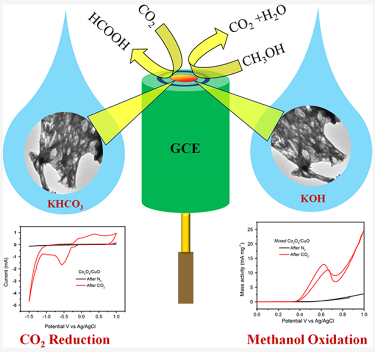

■ INTRODUCTION

Utilization of fossil fuels for energy purposes has been advantageous; however, burning of fossil fuels is associated with the release of undesirable CO_2. Expanding dimensions of CO_2 in the world's climate is of genuine worry that ought to be concerned.[1] High measures of CO_2 in air radically change the temperature of the earth's atmosphere. The anthropogenic carbon dioxide in the atmosphere of the earth will not only increase the worldwide temperature but also oblige the usage of the fossil fuels. It is important to have potential and judicial usage of environmental CO_2. Carbon dioxide present in our environment is a potential source to restore carbon into fuels and other synthetic compounds such as methanol, formaldehyde, formic acid, and so forth.[1−4] In the past few decades, electrocatalytic carbon dioxide reduction has been a potential and sustainable way in combating environmental energy challenges. Our major concern should be not only to restrict the production of CO_2 in the earth's atmosphere and its conversion into potential fuels but also to search the sources other than fossil fuels for energy production. To combat the environmental challenges, use of green and pollutant-free sources is highly appreciated. In this regard, our focus of interest should be on fuel cells and metal−air batteries.

Metal−air batteries and fuel cells have been showing great reliability and promise for automotive industries. Moreover, metal−air batteries and power modules (fuel cells) have demonstrated an incredible guarantee for vehicle enterprises. Fuel cell-based batteries working at extremely lower temperatures are of great interest. In this context, methanol-based fuel cells (DMFCs) have achieved potential consideration as they work at extremely low temperatures (−150 °C).[5,6] This makes DMFCs potential equipment to be utilized in electric devices and vehicles in remote locations having extremely cold climatic situations. In DMFCs, the chemical species with a high hydrogen-to-carbon ratio are produced during methanol oxidation. These chemical species give rise to production of enormous hydrogen, which is utilized as an input energy source in fuel cells.[7] The final product of methanol oxidation as expected is carbon monoxide (CO). Formation of CO limits the function of the catalyst life cycle. This hindrance in the

Received: September 2, 2020
Revised: September 25, 2020
Published: October 9, 2020

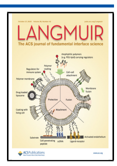

https://dx.doi.org/10.1021/acs.langmuir.0c02554
Langmuir 2020, 36, 12760−12771

Scheme 1. Formation of the Nanosheet through Solution Combustion Synthesis

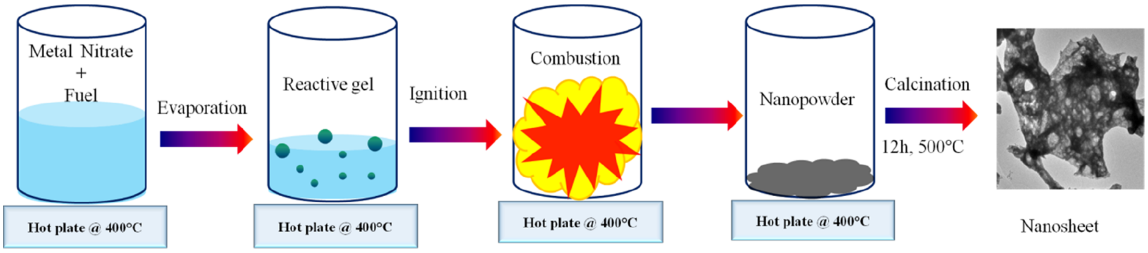

electrocatalysis process of catalysts by the formation of excess CO is known as CO poisoning.[7−10] The other drawback associated with the electrocatalysts is that they work at high overpotentials during methanol dehydrogenation.[11] Pt and Pt-based electrocatalysts have played a pioneering role in overcoming the overpotential concern as they perform methanol dehydrogenation at low overpotentials.[7−11] Despite the good activities of Pt and Pt-based electrocatalysts, they are highly susceptible to CO poisoning and expensive as well. Co and Cu-based electrocatalysts have been pretty successful both in methanol oxidation and in CO_2 reduction.[11−20] Metals and metal oxides of Co and Cu not only are cheap to replace expensive Pt-based fuel cells for commercial purposes but also work at low overpotentials to carry out both the reactions.[11−20] Habermehl-Ćwirzeń and co-workers reveal that the Co(0001) plane plays an important role in the oxidation of methanol *via* dissociative adsorption.[21] Glisenti and Natile studied cobalt oxide surfaces (CoO and Co_3O_4) for methanol oxidation, and they concluded that methanol is molecularly chemisorbed at room temperature with formate and formaldehyde as end products.[22] In the CO_2 conversion case, both metallic and metal oxide-based Cu and Co nanoparticles (NPs) have also shown good performance, especially Cu-based metals and metal oxides are considered as best catalysts in CO_2 reduction. However, unfortunately, Cu-based catalysts face some serious shortcomings such as low selectivity, production of hydrogen as a side product, and poor Faradaic efficiency (FE).[17] To overcome these shortcomings, there have been good attempts to ameliorate the activity of CO_2 conversion and selectivity. One of these attempts is to utilize the concept of the synergistic effect *via* designing of Cu-based alloys such as the Au−Cu, In−Cu, Sn−Cu, Pd−Cu, Ag−Cu, and Ni−Cu types.[17] Reports have inferred that the CoCu alloy is a better electrocatalyst than individual Cu NPs.[19,20] Mayrhofer and co-workers studied the CoCu alloy, and they concluded that there is a drastic change in selectivity and activity in CO_2 conversion when Co contents are mixed with Cu.[19] Based on these assumptions, here, we proposed the synthesis of the Co_3O_4 nanosheet (NS), the CuO NS, and mixed CO_3O_4/CuO nanocomposites to study methanol oxidation and CO_2 conversion. The application results of both methanol oxidation and CO_2 conversion revealed that mixed CO_3O_4/CuO nanocomposites are better electrocatalysts than their individual metal oxides. The main aim of this study was to design pollutant-free, green electrocatalysts viable to generate energy for fuel cell applications, which also shows a promising property of carbon dioxide conversion.

■ EXPERIMENTAL SECTION

The chemicals used were in their purest forms. From Bio-Rad laboratories, $Cu(NO_3)_2{\cdot}3H_2O$ was taken. $Co(NO_3)_2{\cdot}6H_2O$, isopropyl alcohol, $NaBH_4$, and perfluorinated Nafion were purchased from Sigma-Aldrich Company. From Intra-Laboratories, UK, $KHCO_3$ was purchased. Glycine was purchased from VWR chemicals. To prepare all the solutions, deionized Millipore water was used. The nanosheet was prepared through a solution combustion technique as described in Scheme 1. Synthesis of the CuO NS, Co_3O_4NS, and mixed CuO/Co_3O_4 NS is as discussed below.

Synthesis of CuO: Copper oxide (CuO) was prepared through the solution combustion synthesis technique. For this, an aqueous solution of 20 mL containing 8.9 g of copper nitrate ($Cu(NO_3)_2{\cdot}3H_2O$) and 3.08 g of glycine ($C_2H_5NO_2$) was taken in a 100 mL container. The precursor amounts were calculated for the synthesis of 3 g of the nanopowder by following a reported literature.[23] The fuel-to-oxidizer ratio was taken as 1. In order to dissolve the metal precursors, the mixture was sonicated for 15 min. After following this procedure, this homogeneous mixture was kept on a hot plate at 400 °C until the water present got evaporated. Once the whole water got evaporated, self-ignition took place, which triggered combustion reaction inside the beaker, which converted the metal precursor into NPs. These NPs were crushed using a mortar pestle, and the as-obtained powder was sieved through a 100 μm sieve to get a uniform size of particles. After that, the sample was kept in a crucible and was given heat treatment for 12 h at 500 °C.

Synthesis of Co_3O_4: The same procedure as above was followed, but instead of copper nitrate, 3.49 g of cobalt nitrate ($Co(NO_3)_2{\cdot}6H_2O$) and 1 g of glycine were taken.

Synthesis of mixed CuO/Co_3O_4: The same methodology as above was followed. However, both metal precursors cobalt nitrate (2.61 g) and copper nitrate (2.169 g) were taken. The glycine amount here was considered as 1.5 g.

The stoichiometric theoretical reaction for combustion, under equilibrium, is generally written as[24]

$$\begin{aligned} &Me^{v}(NO_3)_v + 5/9v\varphi NH_2CH_2COOH + 5/4v(\varphi - 1)O_2 \\ &\rightarrow MeO_{v/2} + 10/9v\varphi CO_2 + 25/18v\varphi H_2O \\ &+ \{(5\varphi + 9)/18\}vN_2 \end{aligned}$$

where Me^v is the metal with valence v and φ is the fuel-to-oxidizer ratio.[25] $\varphi = 1$ indicates no requirement of oxygen for the initial mixture to completely oxidize the fuel, while $\varphi > 1$ (<1) indicates fuel-rich (lean) conditions. For the solution combustion synthesis of metal oxides, the $\varphi = 1$ stoichiometry is taken into account. Mostly for the stoichiometric $\varphi = 1$ condition, metal oxides are formed but depend on the type of metal nitrate precursor used as well. For the fuel-rich ($\varphi > 1$) or fuel-lean ($\varphi < 1$) condition, we may expect different products. Hence, we believe synthesis of the Co_3O_4/CuO NS depends on the φ value, so tuning of composition seems to be limited.

Techniques for Characterization. To examine the structure of CuO, Co_3O_4, and mixed Co_3O_4/CuO crystals, an X-ray powder diffractometer, a PANalytical model with CuKαCuKα radiation with a wavelength of 1.5418 Å, was used. Morphological studies of the electrocatalysts CuO, Co_3O_4, and mixed Co_3O_4/CuO were evaluated using high-resolution scanning electron microscopy (SEM) (Nova Nano 450, FEI Waltham, MA, USA), and transmission electron microscopy (TEM) analysis of CuO, Co_3O_4, and mixed Co_3O_4/CuO

https://dx.doi.org/10.1021/acs.langmuir.0c02554
Langmuir 2020, 36, 12760−12771

was carried out using high-resolution TEM (HRTEM), Tecnai G2. Carbon-coated Ni grids (400-mesh) were used for TEM analysis of CuO, Co_3O_4, and mixed Co_3O_4/CuO. Water/ethanol solution was used for dispersion of samples. X-ray photoelectron spectroscopy (XPS, Kratos AXIS Ultra DLD, Manchester, UK) was employed to examine oxidation states and the surface composition of the CuO, Co_3O_4, and mixed Co_3O_4/CuO NSs.

Electrode Preparation. To examine the efficiency of the CuO, Co_3O_4, and mixed Co_3O_4/CuO NSs, an ink containing 100 μL of isopropyl alcohol, 5 mg of the catalyst powder, 40 μL of Nafion (5%) solution, and 40 μL of deionized water was prepared. After 15 min sonication (in a glass vial with a volume of 10 mL), an amount of volume equal to 5 μL was drop-cast on a glassy carbon electrode (GCE). KOH (1 M) and 0.5 M $KHCO_3$ electrolytes were employed to carry out electrochemical measurements for methanol oxidation and CO_2 reduction, respectively.

■ RESULTS AND DISCUSSION

The preparation and synthetic procedure of the CuO, Co_3O_4, and mixed Co_3O_4/CuO electrocatalysts are well discussed in the Experimental Section. In brief, the CuO, Co_3O_4, and mixed Co_3O_4/CuO electrocatalysts were synthesized through the solution combustion technique, followed by calcination.

Powder X-ray diffraction (PXRD) was done to study the crystalline nature of the Co_3O_4, CuO, and mixed Co_3O_4/CuO electrocatalysts (Figure 1). The PXRD pattern of CuO depicts

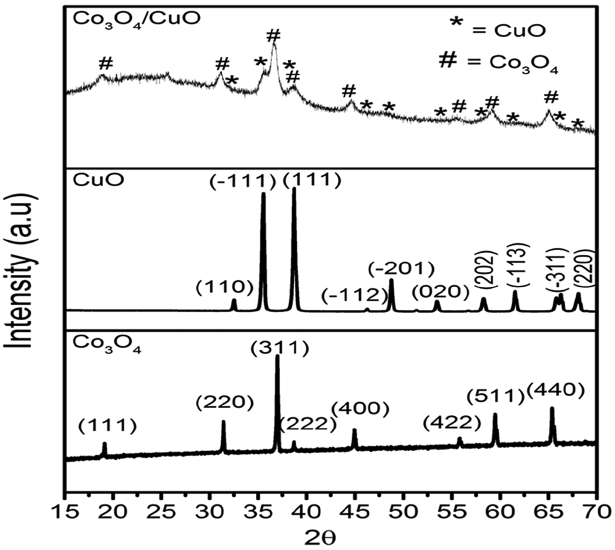

Figure 1. PXRD patterns of the Co_3O_4, CuO, and mixed Co_3O_4/CuO electrocatalysts. The 2θ values from 10 to 80° with a scan rate of 2° per min were considered during PXRD measurement.

peaks with 2θ values of 32.49, 35.48, 38.74, 46.28, 48.76, 53.58, 58.31, 61.58, 66.24, and 68.08°, which correspond to the (110), (−111), (111), (−112), (−202), (020), (202), (−113), (−311), and (220) crystal planes, respectively. This type of crystal structure represents a monoclinic phase of CuO. This crystal structure exhibits diffraction peaks which perfectly match with the information given in JCPDS data (80-0076). The crystal pattern of Co_3O_4 shows diffraction peaks at 19.18, 31.48, 36.96, 38.63, 44.89, 55.70, 59.42, and 65.36°, which can be indexed to the (111), (220), (311), (222), (440), (422), (511), and (440) planes of Co_3O_4 (JCPDS file no. 42-1467), respectively. This type diffraction pattern of Co_3O_4 represents a cubic spinel structure. The crystal pattern of mixed Co_3O_4/CuO nanocomposites shows diffraction peaks at 19.14, 31.14, 32.24, 35.51, 36.76, 38.16, 38.79, 44.56, 46.13, 48.32, 53.92, 55.64, 58.13, 59.23, 61.25, 65.02, 66.10, and 67.99°, which can be indexed to the (111), (220), (110), (−111), (311), (111), (222), (400), (−112), (−201), (020), (422), (202), (511), (−113), (440), (−311), and (220) planes, respectively. Co_3O_4/CuO planes (110), (−111), (111), (−112), (−202), (020), (202), (−113), (−311), and (220) can be indexed to CuO, and crystal planes (111), (220), (311), (222), (440), (422), (511), and (440) are due to Co_3O_4. The oxidation states of the mixed oxide Co_3O_4/CuO electrocatalyst was evaluated by performing XPS experiments. The Co 2p core-level spectrum (Figure 2a) shows two characteristic significant peaks of Co_3O_4 with binding energies (BEs) of 780.64 and 796 eV, which correspond to the Co $2p_{1/2}$ and Co $2p_{3/2}$ signals, respectively.[24] The energy of orbital splitting is equal to 15.35 eV, and both of the signals authenticate the existence of Co^{2+} and Co^{3+}. The presence of a doublet with BEs of 783 and 797.6 eV reflects the possibility of surface $Co(OH)_2$ NPs.[26]

The Cu 2p core-level spectrum (Figure 2b) shows significant peaks of CuO with BEs of 934 and 953.98 eV, which are attributed to the Cu $2p_{3/2}$ and Cu $2p_{1/2}$, signals, respectively.[27] There also exist three shake-up satellite signals at 942.49, 944, and 962.68 eV.[27,28] The well-intense shake-up satellite signal confirms the presence of the Cu^{2+} oxidation state and rules out the presence of the Cu_2O phase. In addition to this, the O 1s XPS spectrum (Figure 2c) represents a significant peak at 530.07 eV, which authenticates the presence of oxygen in Co_3O_4/CuO and the broad signal at 532 eV signifies the possibility of $Cu(OH)_2$ and $Co(OH)_2$ on the surface.[28,29] The survey spectrum is shown in Figure S1. The peaks corresponding to BEs at 713 and 644 eV are Auger peaks of Co and Cu, respectively. SEM analysis was done in order to study the shape and morphology of the Co_3O_4, CuO, and mixed Co_3O_4/CuO electrocatalysts. SEM images of the Co_3O_4, CuO, and mixed Co_3O_4/CuO electrocatalysts are shown in Figure 3a, b, and c, respectively.

The information that is reflected by SEM images is a porous fibrous structure of the Co_3O_4, CuO, and mixed Co_3O_4/CuO electrocatalysts with uniform consistency.

The TEM images shown in Figure 4 show a sheetlike morphology of the mixed Co_3O_4/CuO nanostructure. To examine the arrangement in the Co_3O_4 and CuO crystal planes, the HRTEM technique was employed, as shown in Figure 4b. The lattice fringes with interplanar spacings of "*d*" = 0.53 and 0.245 nm correspond to the (−111) plane of CuO and the (311) plane of Co_3O_4, respectively. This information matches well with the XRD results. The TEM images of CuO and Co_3O_4 alone are shown in Figure S2. The adsorption/desorption of nitrogen through BET analysis to analyze the surface area (SA) and porosity of Co_3O_4/CuO is shown in (Figure 5). Energy-dispersive X-ray spectra are shown in Figure S3, and they convey the information of the presence of the copper and cobalt phases along with oxygen. From BET analysis, it was confirmed that the SA and pore volume of Co_3O_4/CuO are 50.026 m^2 g^{-1} and 0.201762 cm^3 g^{-1}, respectively. The pore diameter was also detected to be 80.7 Å, which indicates the microporous nature of Co_3O_4/CuO. The shape of the isotherm also conveys the presence of micropores. The porosity of Co_3O_4 and CuO is given in S4 and S5, respectively. The comparison of the SA, pore volume, and pore diameter of the CuO, Co_3O_4, and Co_3O_4/CuO NSs is given in Table 1. The comparative details show that the SA of CuO =

https://dx.doi.org/10.1021/acs.langmuir.0c02554
Langmuir 2020, 36, 12760−12771

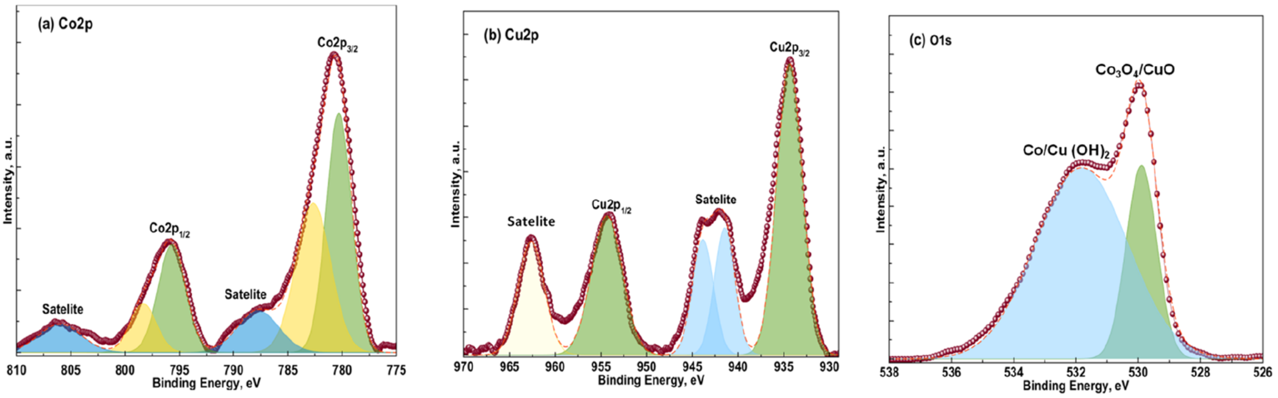

Figure 2. (a) XPS diagram showing BE levels of the Co_3O_4 phase of mixed Co_3O_4/CuO. (b) BE levels of the CuO phase of mixed Co_3O_4/CuO. (c) BE of oxygen.

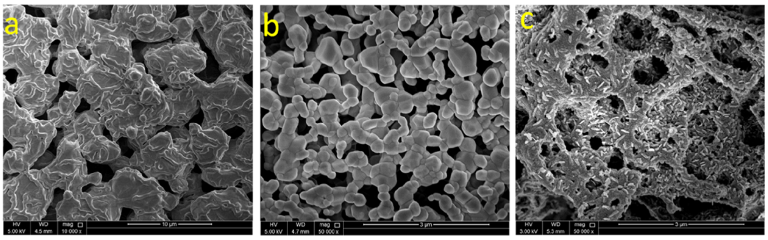

Figure 3. Field emission SEM images of Co_3O_4, CuO, and mixed Co_3O_4/CuO.

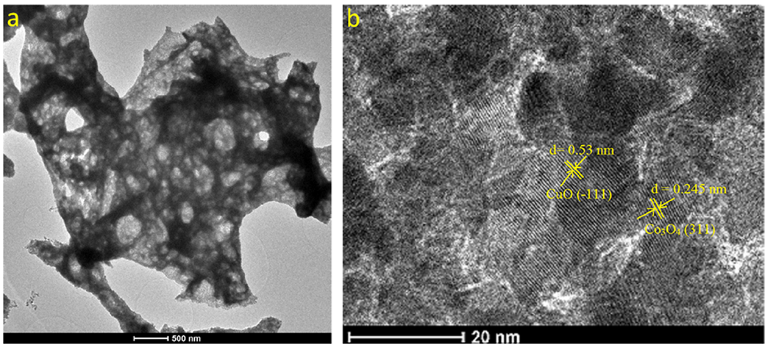

Figure 4. (a) TEM image and (b) HRTEM image of mixed Co_3O_4/CuO.

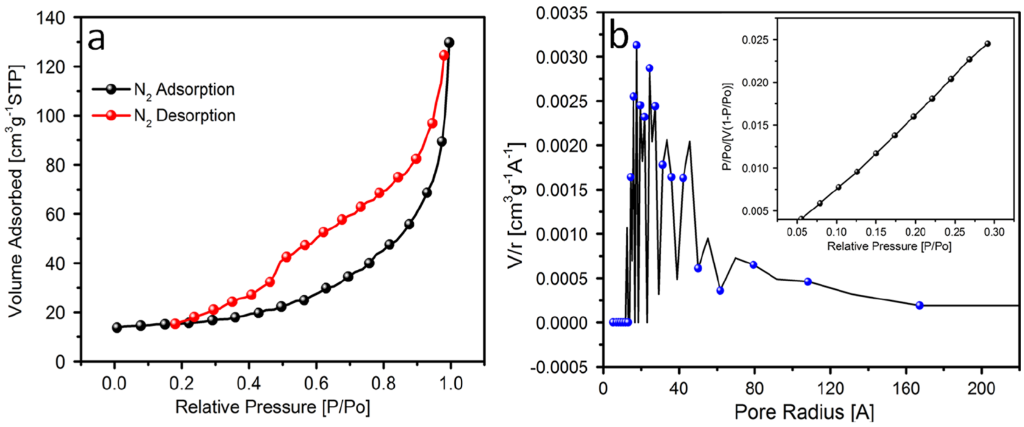

Figure 5. (a) BET nitrogen adsorption isotherm plot of the Co_3O_4/CuO NS. (b) BET SA and pore size distribution of the Co_3O_4/CuO NS.

https://dx.doi.org/10.1021/acs.langmuir.0c02554
Langmuir 2020, 36, 12760−12771

Table 1. Comparison of the SA, Pore Volume, and Pore Diameter of the CuO, Co_3O_4, and Co_3O_4/CuO NSs

sr. no	nanosheet	surface area (m^2 g^{-1})	pore volume (cm^3 g^{-1})	pore diameter (Å)
1	CuO	10.161	0.038126	75.0
2	Co_3O_4	3.603	0.017922	99.5
3	Co_3O_4/CuO	50.026	0.201762	80.7

10.16 m^2/g, Co_3O_4 = 3.6 m^2/g, and Co_3O_4/CuO = 50.03 m^2/g. Hence, the Co_3O_4/CuO NS has 4.9 times more SA than the CuO NS and 13.97 times more SA than the Co_3O_4 NS.

Application in Methanol Oxidation. Cyclic voltammograms were examined by employing a three-electrode system bipotentiostat (Pine Research Instruments). The GCE as the working electrode, Ag/AgCl as the reference electrode, and a graphitic rod as the counter electrode were utilized to carry out all the electrochemical measurements. For the methanol oxidation reaction (MOR), a 0−1 V versus Ag/AgCl potential widow was selected. In the MOR study, a 5 mV s^{-1} scan rate was employed for every electrochemical measurement in the GCE-modified CuO, Co_3O_4, and mixed Co_3O_4/CuO electrodes. The cyclic voltammetry (CV) run of the CuO, Co_3O_4, and mixed Co_3O_4/CuONS electrodes in saturated N_2 and 0.5 M methanol solution is shown in Figure 6a−c. The polarization increase in the direction of the anode was taken from 0 to 1 V, and from there, the potential applied was changed to 1−0 V in the direction of the cathode. The black curves of Figure 6a−c indicate the absence of any characteristic peak in the potential region of 0−1 V after N_2 purge and the absence of methanol for CuO, Co_3O_4, and mixed Co_3O_4/CuO-modified GCE, thus reflecting no MOR activity. After methanol addition (0.5 M), the appearance of a well-intense anodic peak at 0.62 V and the increase in density of current reflect that the CuO, Co_3O_4, and mixed Co_3O_4/CuO electrocatalysts have a role in the oxidation of methanol. Figure 7a shows a comparison of all the three catalysts. The information obtained from Figure 7a conveys that under similar conditions (0.5 M methanol and 1 M KOH), the hybrid Co_3O_4/CuO NS has a corresponding increase in density of current as well as an intense peak at 0.62 V. Hence, the hybrid Co_3O_4/CuO NS is more active among the three catalysts, followed by Co_3O_4, with the least activity in the case of the CuO electrocatalyst.

The mass activity of the mixed Co_3O_4/CuO NS produced at 0.627 V versus Ag/AgCl during methanol oxidation (0.5 M) was 12 mA g^{-1}, which is 2.4 times better than that of Co_3O_4, whose mass activity is 5 mA g^{-1}, and 4 times better than that of the CuO NS, whose mass activity is 3 mA g^{-1}. The MOR activity of CuO, Co_3O_4, and mixed Co_3O_4/CuO was also assessed at a 1 M concentration of methanol, and the same trend was experienced as shown in Figures S6 and S7, and mixed Co_3O_4/CuO showed better activity than the Co_3O_4 and CuO electrocatalysts here as well. All the three electrocatalysts displayed higher mass activity and current density values as compared to the results displayed in the 0.5 M methanol concentration. The electrocatalytic performance (mass activity and specific activity) of our electrocatalysts (the CuO NS, Co_3O_4 NS, and Co_3O_4/CuO NS) toward MOR with two different concentrations (0.5 and 1 M) of methanol is given in Table 2. Some extra CV measurements were carried out in order to determine MOR rate dependency on methanol concentrations. This was done by changing the methanol concentration from 0.5 to 2.5 M under similar parameters (1 M KOH and 5 mV s^{-1}). From Figure 7b, the increase in density of current with methanol concentration increase can be inferred. The current density values that were taken to study the rate of the reaction were 7.70 mA/cm^2 (at 0.62 V), 12.44 mA/cm^2 (at 0.76 V), 15.30 mA/cm^2 (at 0.86 V), and 19.74 mA/cm^2 (at 0.94 V), corresponding to 0.5, 1, 1.5, and 2.5 M methanol concentrations, respectively. As shown in Figure 7c, the slope apparently follows a linear trend with the slope equal to 0.56. This indicates first-order dependency of the reaction with methanol concentration. We also checked the stability of our Co_3O_4/CuO NS using the chronoamperometry technique (Figure 7d). The data current versus time was recorded at a fixed potential of 0.6 V versus Ag/AgCl in 0.5 M methanol and the 1 M KOH solvent. We find out that the catalyst is stable for more than 12 h. However, we realize that there was a decrease in current density with time. Post electrocatalytic methanol oxidation, the sample was collected from the surface of the GCE electrode, and SEM and TEM characterization were done again. Figures S8 and S9 reveal that the Co_3O_4/CuO NS has retained the morphology after methanol oxidation, and this also gives confirmation of stability of the Co_3O_4/CuO NS. The comparison of the Co_3O_4/CuO NS with Pt/C-, copper-, and cobalt-based transition-metal oxide electrocatalysts toward methanol electro-oxidation in alkaline media is given in Table 3.

Application in CO_2 Conversion. CuO, Co_3O_4, and mixed Co_3O_4/CuO were applied for the electrocatalytic conversion of carbon dioxide. A rotating ring-disc electrode (RRDE) was employed to carry out all the experiments. CV scans were studied in a potential window region of 0.8 to −1.2 V versus

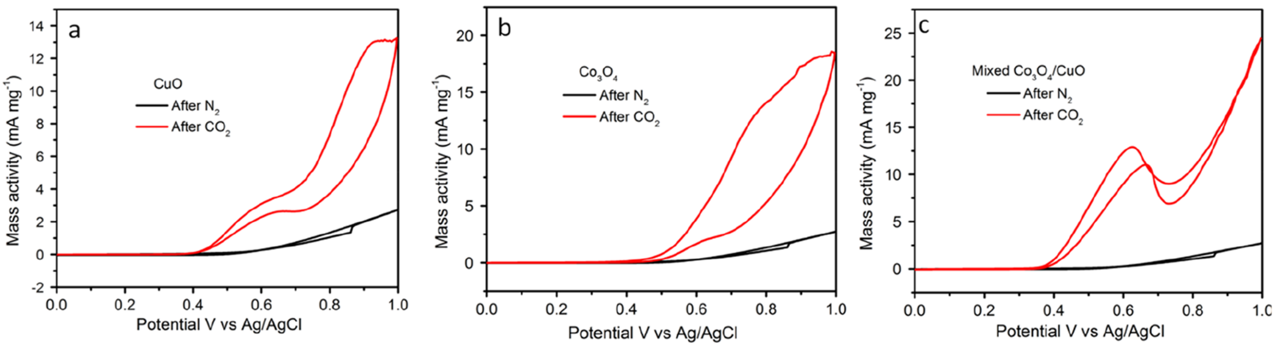

Figure 6. CV diagram showing mass activity of (a) CuO, (b) Co_3O_4, and (c) mixed Co_3O_4/CuO after N_2 purge (the black curve) and 0.5 M methanol (the red curve).

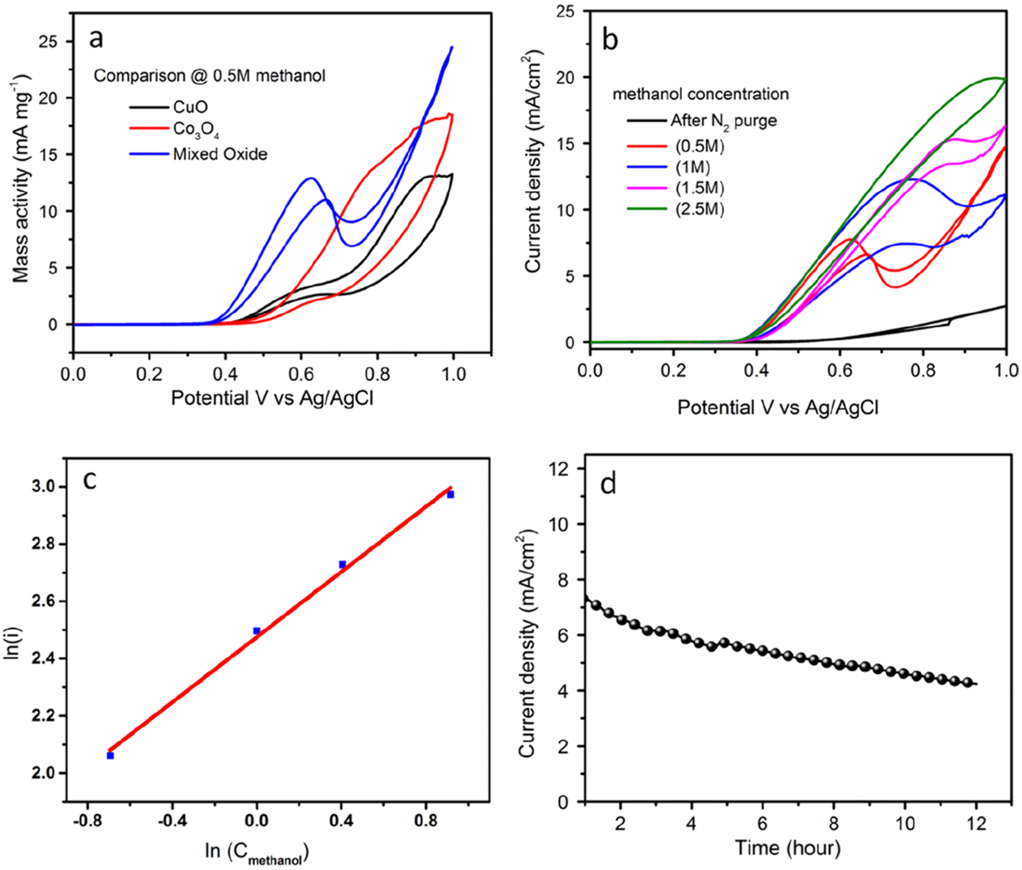

Figure 7. (a) CV diagram showing the comparative study of CuO, Co_3O_4, and mixed Co_3O_4/CuO after N_2 purge and methanol (0.5 M). (b) CV diagram showing the activity of mixed Co_3O_4/CuO at different methanol concentrations. (c) Logarithmic-scale representation of density of current (mA/cm^2) vs concentration of methanol (M). (d) Chronoamperometry check of the Co_3O_4/CuO NS at the fixed potential of 0.6 V vs Ag/AgCl in 0.5 M methanol and the 1 M KOH solvent up to 12 h.

Table 2. Electrocatalytic Performance of Our Electrocatalysts (the CuO NS, Co_3O_4 NS, and Co_3O_4/CuO NS) toward MOR Activity in Alkaline Media with Two Different Concentrations (0.5 and 1 M) of Methanol

sr. no.	catalyst	electrolyte (M)	at a fixed potential (V) vs Ag/AgCl	scan rate	mass activity mA g^{-1}	specific activity mA cm^{-2}
1	CuO NS	KOH: 1 CH_3OH: 0.5	0.627	5	3	1.2
2	Co_3O_4 NS	KOH: 1 CH_3OH: 0.5	0.627	5	5	1.5
3	Co_3O_4/CuO NS	KOH: 1 CH_3OH: 0.5	0.627	5	12	6.07
4	CuO NS	KOH: 1 CH_3OH: 1	0.77	5	4.7	2.9
5	Co_3O_4 NS	KOH: 1 CH_3OH: 1	0.77	5	5.2	3.2
6	Co_3O_4/CuO NS	KOH: 1 CH_3OH: 1	0.77	5	19.46	12

Ag/AgCl. All the CV scans of the CuO-, Co_3O_4-, and hybrid Co_3O_4/CuO-modified GCEs were analyzed in 0.5 M $KHCO_3$ at a constant scan rate of 25mV s^{-1} (Figure 8). Figure 8a−c represents the activity of the CuO, Co_3O_4, and mixed Co_3O_4/CuO electrocatalysts after N_2 and CO_2 purge. Figure 8a−c infers that the cathodic current dramatically increases in the solution saturated with CO_2 after −0.9 V, in comparison to the solution saturated with N_2. Three redox peaks at −0.1 and 0.3 V in the forward direction and one redox peak at −0.7 V can be seen in reverse scans. The peaks at potentials of −0.1 and −0.7 V versus Ag/AgCl are due to the reduction of Cu(II) oxide (CuO) to Cu(I) oxide (Cu_2O) or Cu(0), and the peak at the potential of 0.3 V versus Ag/AgCl is due to the oxidation of Cu_2O to CuO. The information that is conveyed by these results is that the electrons that come from the cathode are utilized with high efficiency in the CO_2-saturated solution. This consumption of CO_2 results in a dramatic increase in density of current in the potential region of −0.9 to −1 V. Figure 8d shows the relative comparison of the CuO, Co_3O_4, and mixed Co_3O_4/CuO electrocatalysts at 25 mV/s toward CO_2

https://dx.doi.org/10.1021/acs.langmuir.0c02554
Langmuir 2020, 36, 12760−12771

Table 3. Electrocatalytic Performance of Copper-Based Transition-Metal Oxide Electrocatalysts toward Methanol Electro-Oxidation in Alkaline Media

sr. no.	catalyst	method	electrolyte (M)	potential range (V)	scan rate mV/s	mass activity mA g^{-1}/specific activity mA cm^{-2}	refs
1.	Pt/C	chemical reduction	KOH: 1 CH_3OH: 1	−0.8 to 0.3 V/Hg/HgO	5	-/40	30
2.	Ni−Cu−P/C	electroless deposition	KOH: 0.1 CH_3OH: 0.5	0−1.2 V/Hg/HgO	10	-/9.5	31
3.	Cu/P(2ADPA)/MCPE	polymerization/electrodeposition	NaOH: 0.2 CH_3OH: 0.005	−0.2 to 1.0 V Ag/AgCl	10	-/46	32
4.	platelike Cu particle	Electrodeposition	NaOH: 0.1 CH_3OH: 01	0−1.0 V/SCE	10	-/8.3	33
5.	CuNW@RGO−GCE	Hydrothermal	NaOH: 01 CH_3OH: 1	−0.2 to 1.2 V Ag/AgCl	50	-/1.11	34
6.	Cu−CeO_2/Cu	Electrodeposition	NaOH: 0.1 CH_3OH: 0.8	0−1.6 V/Ag/AgCl	30	-/6.8	35
7.	CoCu/CNF	electrospinning	KOH: 1 CH_3OH: 2	0−0.8 V/Ag/AgCl	50	-/18	36
8.	Cu NP	electrodeposition	NaOH: 0.5 CH_3OH: 0.5	−0.8 to 1.2 V/SCE	50	-/196 at 0.83 V -/80 at 0.6 V	37
9.	RGO−$NiCo_2O_4$	hydrothermal method	KOH: 1 CH_3OH: 0.5	0−0.8 V/Ag/AgCl	50	-/45	38
10.	*meso*-CoPi	liquid crystal template	KOH: 1 CH_3OH: 1	0.0−0.7 V/SCE	50	1512/225	39
11.	*meso*-CoPi	microwave	KOH:1 CH_3OH: 1	0.2−0.7 V/SCE	50	846/126	40
12.	rGO/CuNPs-PT/G	electropolymerization	NaOH: 0.1 CH_3OH: 0.02	−0.1 to 1.4 V/SCE	10	-/16	41
13.	CoCu/CNF	electrospinning	KOH: 1 CH_3OH: 2	−0.2 to 1.0 V/Ag/AgCl	100	-/190 at 1 V -/75 at 0.6 V	42
14.	$CuCo_2O_4$	hydrothermal	KOH: 1 CH_3OH: 0.5	0−0.6 V/SCE	10	27.6 A g^{-1}/-	43
15.	CuO	RF sputtering	KOH: 1 CH_3OH: 0.5	0−0.5 V/SCE	10	29.41 A g^{-1}/10	44
16.	Cu_2O	RF sputtering	KOH: 1 CH_3OH: 0.5	0−0.5 V/SCE	10	3.81 A g^{-1}/6.1	44
17	$Cu(OH)_2$/CuO nanowires	chemical oxidation	KOH: 1 CH_3OH: 0.5	0−0.6 V/SCE	10	55 A g^{-1}/110	45
18	Co_3O_4/CuO NS	combustion method	KOH: 1 CH_3OH: 0.5	0−1 V vs Ag/AgCl	5	12/6.07 at 0.62 V	this work
19	Co_3O_4/CuO NS	combustion method	KOH: 1 CH_3OH: 1	0−1 V vs Ag/AgCl	5	19.46/12 at 0.77 V	this work

reduction activity. From Figure 8d, it can be inferred that the Co_3O_4/CuO electrocatalyst shows better activity than the CuO and Co_3O_4 electrocatalysts. The current density at −1.5 V jumps to −24 mA/cm^2 for Co_3O_4/CuO, which is more than 0.6 times the value for CuO, which is −15 mA/cm^2, and more than 3 times the value for Co_3O_4, which is 8 mA/cm^2. For CO_2 reduction, metallic Cu and Cu-based oxides and hydroxides are considered as state-of-the-art catalysts in CO_2 reduction. Kenis and co-workers reported synthesis of the Cu(core)/CuO-(shell) catalyst for electrocatalytic CO_2 reduction.[46] They revealed that at the potential of −1.35 V versus Ag/AgCl, the current density was 17.3 mA/cm^2. Our group also reported Co/Cu hydroxide NPs on the carbon nitride surface for CO_2 reduction into formate, and we observed the current density of 2.092 mA/cm^2 at a potential of −1.2 V.[47] In this work, the current density recorded at a potential of −1.35 V versus Ag/

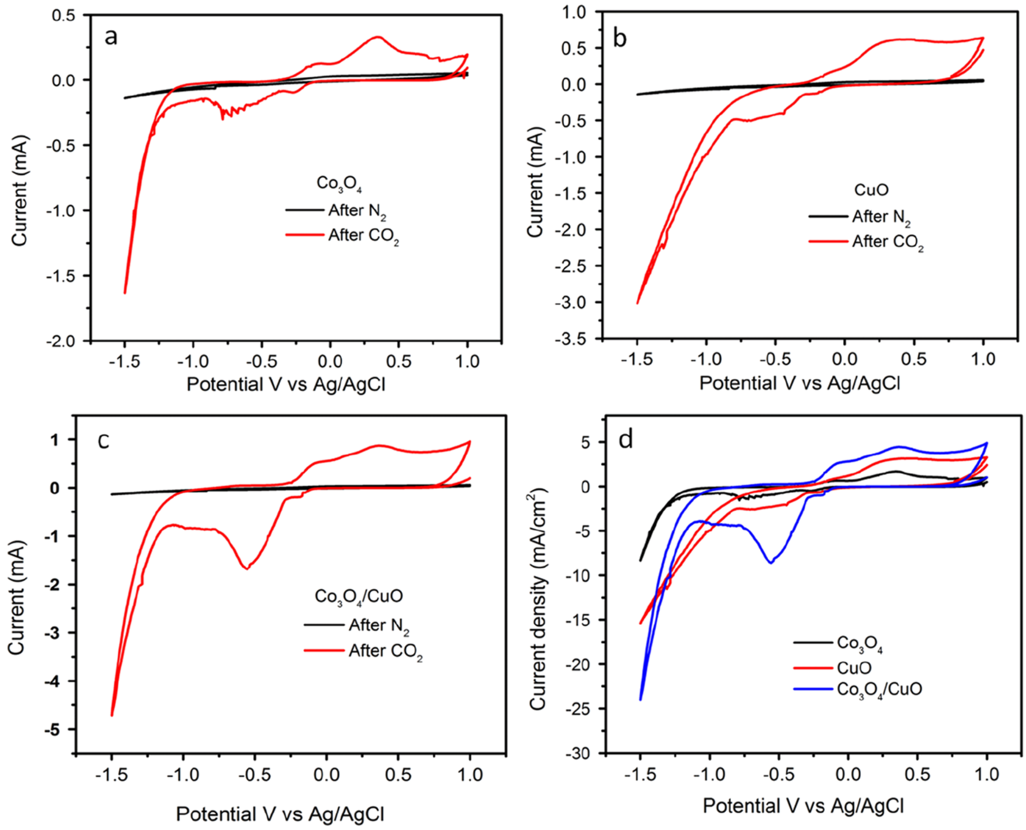

Figure 8. Cyclic voltammogram showing the study of (a) Co_3O_4, (b) CuO, and (c) mixed Co_3O_4/CuO after N_2 purge and methanol (0.5 M) in 0.5 M $KHCO_3$. (d) Cyclic voltammogram showing comparative activity of Co_3O_4, CuO, and mixed Co_3O_4/CuO of methanol (0.5 M) in 0.5 M $KHCO_3$.

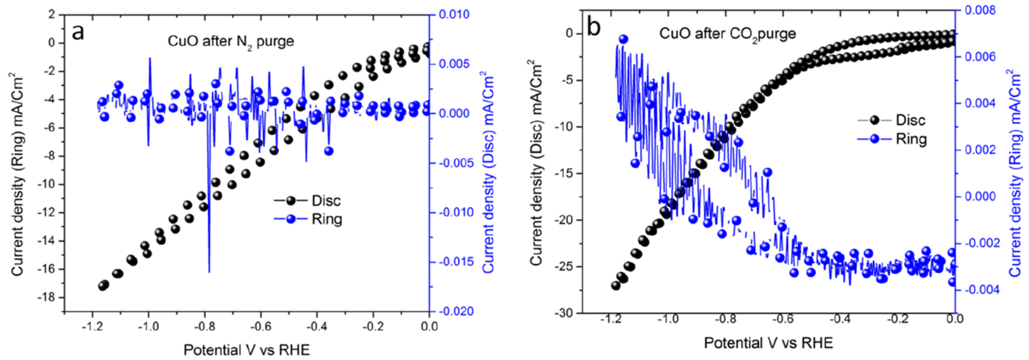

Figure 9. CV scans of CuO in 0.5 M $KHCO_3$ with the RRDE. (a) Electrolyte saturated with nitrogen and (b) electrolyte saturated with CO_2. A scan rate of 100 mV s^{-1} and a rotation of 1500 rpm were carried out for both experiments.

AgCl is 13 mA/cm^2 (Figure 8c), which is comparable to the results reported with various Cu-based catalysts.

Detection of Products. The Co_3O_4-, CuO-, and mixed Co_3O_4/CuO-modified GCEs are primary electrodes, and Pt ring behaves as the secondary working electrode. The product formed on the GCE (formate) is oxidized on the secondary electrode. The role of the secondary electrode is to detect the product formed on the glassy carbon disc (the primary electrode). The catalyst amount in our case (0.17 g) is extremely low, so the product formed is relatively low. The product formed gets dissolved in the bulk of the electrolyte phase. However, as the ring electrode is closer to the disc electrode, the probability of the product near the ring electrode is very high compared to the bulk. The Pt ring electrode oxidizes formate (the product formed on the ring) back into CO_2 and thus authenticates the formation of formate from CO_2 conversion on the disc electrode. The Pt electrode is an excellent choice for the secondary electrode and has been widely used to study oxidation potentials of various CO_2 conversion products such as HCHO, CO, CH_3OH, HCOOH, and so forth. The convenient way to detect the expected product is to monitor the scanning of the disc and give the ring a known oxidation potential of the product. Similarly, the disc is kept at the fixed CO_2 reduction potential

https://dx.doi.org/10.1021/acs.langmuir.0c02554
Langmuir 2020, 36, 12760−12771

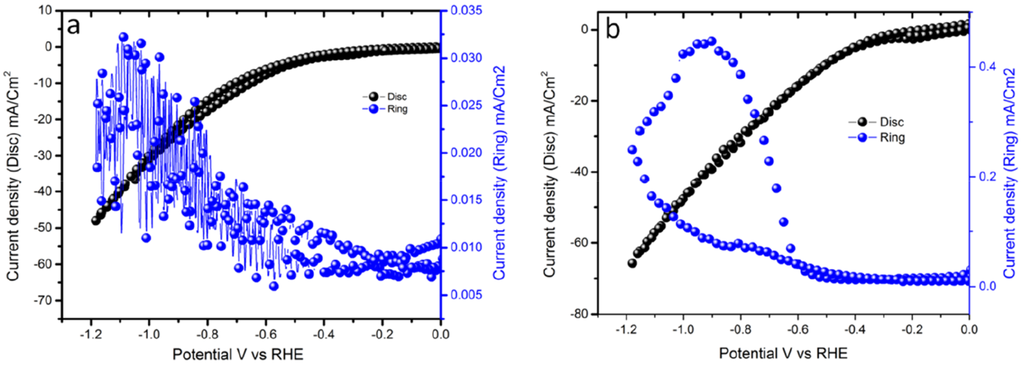

Figure 10. CV scans of Co_3O_4/CuO in 0.5 M $KHCO_3$ with the RRDE. (a) Electrolyte saturated with nitrogen and (b) electrolyte saturated with CO_2. A scan rate of 100 mV s^{-1} and a rotation of 1500 rpm were carried out for both experiments.

(so as to get the maximum product), and the ring is scanned to detect the product formed at the applied disc potential. The Co_3O_4 electrocatalyst was not used to detect the products because of poor activity toward CO_2 reduction, as proved above. However, CuO- and mixed Co_3O_4/CuO-modified GCE electrodes were run in the potential window of 0 to −1.2 V versus the reversible hydrogen electrode (RHE), and the ring electrode was given a potential of 0.9 V versus RHE, which is considered as the formic acid oxidation potential on the Pt ring.[26,28,47,48] Rotating ring disc cyclic voltammetry curves (RRCV) results are shown in Figure 9a,b in N_2- and CO_2-saturated solutions with the CuO electrode. The information that is inferred from Figure 9b conveys a dramatic increase in density of current of both the ring and disc electrodes in comparison to the N_2-saturated solution (Figure 9a). A well-intense peak at −0.9 V (Figure 9b) on the ring electrode authenticates the formate formation. Similarly, RRCV results are shown in Figure 10a and b with the Co_3O_4/CuO-modified GCE after N_2 and CO_2 purge. Similar to the CuO electrode, there was a dramatic increase in the density of current for the disc as well as ring electrodes, but as compared to the CuO electrode, the ring current density of Co_3O_4/CuO was far more superior to that of CuO. Our results are in perfect harmony with the existing results.[46,47] Cu-based catalysts have achieved admirable efficiency for CO_2 conversion and are believed to be excellent catalysts for CO_2 reduction.[17] However, poor FE, low selectivity, and generation of hydrogen as a competitive reaction for CO_2 reduction are some of the shortcomings that the scientific community needs to focus on. Similar to Cu, electrocatalysts of cobalt have also attained satisfactory attention in CO_2 conversion.[18,19] However, reports have revealed that both Cu- and Co-based electrocatalysts have been showing a drastic influence on CO_2 reduction activity and selectivity as well.[19,20] The better activity of the Co_3O_4/CuO NS can be credited to the synergistic effect (mixing of crystal planes) between the Co_3O_4 and the CuO metal oxides, which make the Co_3O_4/CuO NS different from its individual oxides. The synergistic effect in the Co_3O_4/CuO NS makes it a better candidate, resulting in an optimum adsorbate−substrate interaction to facilitate the oxidation/reduction reactions. The synergistic effect has an important role on the activity and stability of our hybrid catalyst CO_3O_4/CuO NS. Besides the synergistic effect, the high SA can be another reason for the better activity and stability of the Co_3O_4/CuO NS as compared to the individual Co_3O_4 and CuO metal oxides. The comparison of the SA, pore volume, and pore diameter of the CuO, Co_3O_4, and Co_3O_4/CuO NSs as given in Table 1 reveals that the SA of CuO = 10.16 m^2/g, the SA of Co_3O_4 = 3.6 m^2/g, and the SA of Co_3O_4/CuO = 50.03 m^2/g, respectively. Hence, the Co_3O_4/CuO NS has 4.9 times more SA than the CuO NS and 13.97 times more SA than the Co_3O_4 NS. Therefore, we believe that both the synergistic effect and the high surface-to-volume ratio may be the reasons for the better performance of the hybrid material than Co_3O_4 or CuO at 100 mV s^{-1} and a rotation of 1500 rpm. Zhu *et al.* carried out a series of experiments. They gave fixed potential values to the disc starting from −0.4 to −0.9 V while scanning the ring in the potential window of 0−1.3 V.[48] Through these experiments, they concluded that when the disc was given a potential of −0.9 V, the intensity of the oxidation peak was high in comparison to those when fixed potential values of −0.4, −0.5, −0.6, −0.7, and −0.8 V were given. Their results reveal that there is maximum conversion of CO_2 into formate at the disc potential of −0.9 V and the oxidation potential of formate on the ring is 0.9 V. We also repeated the procedure done by the Zhu group with our catalyst Co_3O_4/CuO; we scanned the ring in the potential window of 0−1.3 V and kept the potential of the disc at −0.9 V (Figure 11). From the figure, the peak at 0.9 V authenticates the formation of formate on the surface of Co_3O_4/CuO. Even though there is ample evidence that in our case CO_2 have been converted to formate.

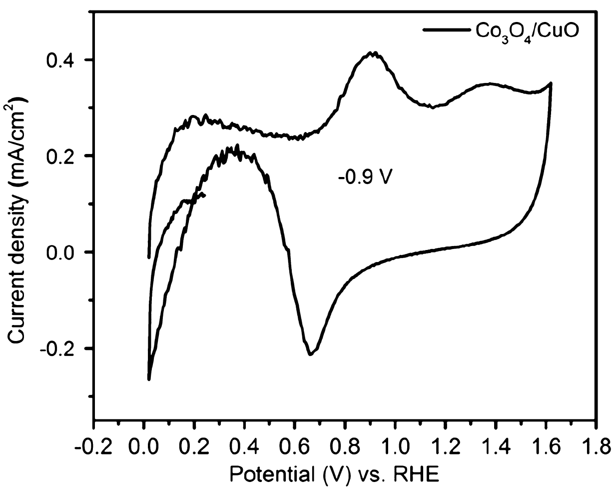

Figure 11. Ring electrode CV scan of Co_3O_4/CuO. A scan rate of 1500 rpm was taken.

https://dx.doi.org/10.1021/acs.langmuir.0c02554
Langmuir 2020, 36, 12760−12771

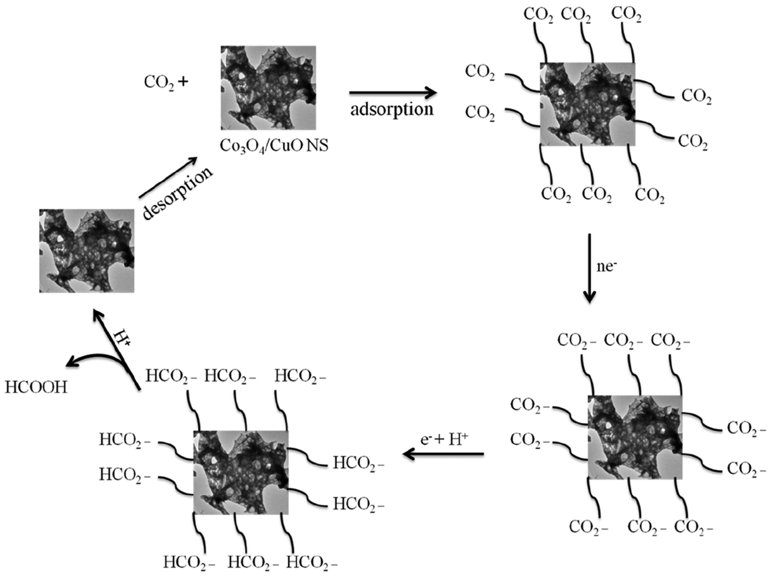

Figure 12. Transformation of CO_2 to HCOOH on the Co_3O_4/CuO surface as a probable mechanism.

However, we can not exclude the formation of hydrogen. Both CO_2 reduction and the hydrogen evolution reaction (HER) are competitive reactions within the same potential region, so production of hydrogen may not be completely excluded. The reports have revealed that there is suppression of HER by 60% when Cu is strained.[28,49] In our case, we believe that there may be strain in Co_3O_4/CuO, which helps in suppression of HER. Figure 12 reveals a probable mechanism for CO_2 conversion into formic acid on the Co_3O_4/CuO surface. Initially, the molecules of CO_2 get adsorbed on the surface of Co_3O_4/CuO. The flow of electrons from the GCE transforms CO_2 molecules into the carbonate anion, and this carbonate anion in the presense of electrons and protons is transformed into the bicarbonate ion.[26,28,47] Then, the conversion of the bicarbonate ion in an acidic medium results in the formation of formic acid, which desorbs from the surface of Co_3O_4/CuO. The efficiency of the Co_3O_4/CuO NS toward methanol oxidation and carbon dioxide reduction can be due to the presence of abundant active sites on edges of the NS, active sites caused due to surface defects and the micropores present in the Co_3O_4/CuO NS. According to Sun *et al.*, sites of atoms at edges of the NS possess unsaturated coordination as well as dangling bonds which decrease the activation energy barrier as well as tend to stabilize the reaction intermediates.[50] Therefore, these edge atoms of NSs which are more exposed to reactant molecules behave as active sites. In addition to this, there are surface defects along the micropores present in NSs that promote the diffusion of reactants and facilitate the formation of products; the atoms present in these micropores are also less coordinated and more exposed to reactants, and hence, these are also considered as active sites. The Co_3O_4/CuO NS is high in SA with the porous nature of the surface, and these micropores including the surface defects and edges of the NS may be the active sites in the hybrid Co_3O_4/CuO NS. In addition to this, CuO and Co_3O_4 interfaces (intercalation of crystal planes) probably are also rich sources of active sites and can be the reason for the better activity of the Co_3O_4/CuO NS.

■ ASSOCIATED CONTENT

Supporting Information

The Supporting Information is available free of charge at https://pubs.acs.org/doi/10.1021/acs.langmuir.0c02554.

XPS survey spectrum of the mixed Co_3O_4/CuO NS; TEM image of Co_3O_4 and CuO; EDS spectra of the Co_3O_4/CuO NS; BET nitrogen adsorption isotherm plot of the Co_3O_4 NS; BET surface area and pore size distribution of the Co_3O_4 NS; BET nitrogen adsorption isotherm plot of the CuO NS; BET surface area and pore size distribution of the CuO NS; cyclic voltammogram showing comperative mass activity of CuO, Co_3O_4, and mixed Co_3O_4/CuO in methanol; cyclic voltammogram showing current density of CuO, Co_3O_4, and mixed Co_3O_4/CuO in methanol; SEM image of Co_3O_4/CuO after methanol activity check; and TEM image of Co_3O_4/CuO after methanol activity check (PDF)

■ AUTHOR INFORMATION

Corresponding Author

Roshan Nazir – *Department of Chemical Engineering, Qatar University, Doha, Qatar; Department of Chemistry, Bilkent University, 06800 Bilkent, Ankara, Turkey;* orcid.org/0000-0001-5995-7710; Phone: +91 7006017128; Email: roshanandrabi@gmail.com

Authors

Alanoud Khalfani – *Department of Chemical Engineering, Qatar University, Doha, Qatar*

Omnia Abdelfattah – *Department of Chemical Engineering, Qatar University, Doha, Qatar*

Anand Kumar – *Department of Chemical Engineering, Qatar University, Doha, Qatar;* orcid.org/0000-0002-9146-979X

Mohammed Ali Saleh Saad – *Department of Chemical Engineering, Qatar University, Doha, Qatar*

Sardar Ali – *Gas Processing Center, Qatar University, Doha, Qatar;* orcid.org/0000-0002-5378-625X

Complete contact information is available at: https://pubs.acs.org/10.1021/acs.langmuir.0c02554

https://dx.doi.org/10.1021/acs.langmuir.0c02554
Langmuir 2020, 36, 12760−12771

Notes

The authors declare no competing financial interest.

■ ACKNOWLEDGMENTS

The authors would like to gratefully acknowledge the financial support from Total Research & Technology Feluy (Grant Number: QUEX-CENG-TRT-17/18) in conducting this research. Total Research Center Qatar is gratefully acknowledged for the coordination of the project. The statements made herein are solely the responsibility of the authors. We would like to acknowledge the Gas Processing Centre for conducting XRD and XPS analysis; also the SEM and TEM analysis was accomplished in the Central Laboratory Unit, Qatar University.

■ REFERENCES

(1) Zhu, W.; Zhang, L.; Yang, P.; Hu, C.; Dong, H.; Zhao, Z.-J.; Mu, R.; Gong, J. Formation of Enriched Vacancies for Enhanced CO2 Electrocatalytic Reduction over AuCu Alloys. *ACS Energy Lett.* **2018**, *3*, 2144−2149.

(2) Shen, Q.; Chen, Z.; Huang, X.; Liu, M.; Zhao, G. High-yield and selective photoelectrocatalytic reduction of CO2 to formate by metallic copper decorated Co3O4 nanotube arrays. *Environ. Sci. Technol.* **2015**, *49*, 5828−5835.

(3) Ahn, S.; Klyukin, K.; Wakeham, R. J.; Rudd, J. A.; Lewis, A. R.; Alexander, S.; Carla, F.; Alexandrov, V.; Andreoli, E. Poly-Amide Modified Copper Foam Electrodes for Enhanced Electrochemical Reduction of Carbon Dioxide. *ACS Catal.* **2018**, *8*, 4132−4142.

(4) Sato, S.; Arai, T.; Morikawa, T.; Uemura, K.; Suzuki, T. M.; Tanaka, H.; Kajino, T. Selective CO2 conversion to formate conjugated with H2O oxidation utilizing semiconductor/complex hybrid photocatalysts. *J. Am. Chem. Soc.* **2011**, *133*, 15240−15243.

(5) Mayrhofer, K. J. J.; Arenz, M. Improvements to the Efficiency and Lifetime of Polymer Electrolyte Membrane Fuel Cells Can Be Realized by Finding More Active and Stable Electrocatalytic Cathode Materials. A Computational Search Has Found Two Such Alloys and Confirmed Their Enhanced Properties Experimentally. *Nat. Chem.* **2009**, *1*, 518−519.

(6) Jung, H.-G.; Hassoun, J.; Park, J.-B.; Sun, Y.-K.; Scrosati, B. An Improved High-Performance Lithium-Air Battery. *Nat. Chem.* **2012**, *4*, 579−585.

(7) Ham, D. J.; Kim, Y. K.; Han, S. H.; Lee, J. S. Pt/WC as Anode Catalyst for PEMFC: Activity and CO Tolerance. *Catal. Today* **2008**, *132*, 117−122.

(8) Sahin, O.; Kivrak, H. A Comparative Study of Electrochemical Methods on Pt-Ru DMFC Anode Catalysts: the Effect of RuAddition. *Int. J. Hydrogen Energy* **2013**, *38*, 901−909.

(9) Chung, D. Y.; Kim, H. I.; Chung, Y. H.; Lee, M. J.; Yoo, S. J.; Bokare, A. D.; Choi, W.; Sung, Y. E. Inhibition of CO Poisoning on Pt Catalyst Coupled with the Reduction of Toxic Hexavalent Chromium in a Dual-Functional Fuel Cell. *Sci. Rep.* **2014**, *4*, 7450.

(10) Ham, D.; Lee, J. Transition Metal Carbides and Nitrides as Electrode Materials for Low Temperature Fuel Cells. *Energies* **2009**, *2*, 873−899.

(11) Jafarian, M.; Mahjani, M. G.; Heli, H.; Gobal, F.; Khajehsharifi, H.; Hamedi, M. H. A study of the electro-catalytic oxidation of methanol on a cobalt hydroxide modified glassy carbon electrode. *Electrochim. Acta* **2003**, *48*, 3423−3429.

(12) Bluhm, H.; Hävecker, M.; Knop-Gericke, A.; Kleimenov, E.; Schlögl, R.; Teschner, D.; Bukhtiyarov, V. I.; Ogletree, D. F.; Salmeron, M. Methanol oxidation on a copper catalyst investigated using in situ X-ray photoelectron spectroscopy. *J. Phys. Chem. B* **2004**, *108*, 14340−14347.

(13) Werner, H.; Herein, D.; Schulz, G.; Wild, U.; Schlögl, R. Reaction pathways in methanol oxidation: kinetic oscillations in the copper/oxygen system. *Catal. Lett.* **1997**, *49*, 109−119.

(14) Zafeiratos, S.; Dintzer, T.; Teschner, D.; Blume, R.; Hävecker, M.; Knop-Gericke, A.; Schlögl, R. Methanol oxidation over model cobalt catalysts: Influence of the cobalt oxidation state on the reactivity. *J. Catal.* **2010**, *269*, 309−317.

(15) Xia, Y.; Dai, H.; Jiang, H.; Zhang, L. Three-dimensional ordered mesoporous cobalt oxides: Highly active catalysts for the oxidation of toluene and methanol. *Catal. Commun.* **2010**, *11*, 1171−1175.

(16) Heli, H.; Jafarian, M.; Mahjani, M. G.; Gobal, F. Electro-oxidation of methanol on copper in alkaline solution. *Electrochim. Acta* **2004**, *49*, 4999−5006.

(17) Ajmal, S.; Yang, Y.; Li, K.; Tahir, M. A.; Liu, Y.; Wang, T.; Bacha, A.-U.-R.; Feng, Y.; Deng, Y.; Zhang, L. Zinc Modified Copper Catalyst for Efficient (Photo-) Electrochemical CO2 Reduction with High Selectivity of HCOOH Production. *J. Phys. Chem. C* **2019**, *123*, 11555−11563.

(18) Park, S.; Kim, Y.; Han, H.; Chung, Y. S.; Yoon, W.; Choi, J.; Kim, W. B. In situ exsolved Co nanoparticles on Ruddlesden-Popper material as highly active catalyst for CO2 electrolysis to CO. *Appl. Catal., B* **2019**, *248*, 147−156.

(19) Grote, J.-P.; Zeradjanin, A. R.; Cherevko, S.; Savan, A.; Breitbach, B.; Ludwig, A.; Mayrhofer, K. J. J. Screening of material libraries for electrochemical CO_2 reduction catalysts−Improving selectivity of Cu by mixing with Co. *J. Catal.* **2016**, *343*, 248−256.

(20) Ghouri, Z. K.; Barakat, N. A.; Kim, H. Y. Influence of copper content on the electrocatalytic activity toward methanol oxidation of Co χ Cu y alloy nanoparticles-decorated CNFs. *Sci. Rep.* **2015**, *5*, 16695.

(21) Habermehl-Ćwirzeń, K.; Lahtinen, J.; Hautojärvi, P. Methanol on Co (0 0 0 1): XPS, TDS, WF and LEED results. *Surf. Sci.* **2005**, *598*, 128−135.

(22) Natile, M. M.; Glisenti, A. Study of surface reactivity of cobalt oxides: interaction with methanol. *Chem. Mater.* **2002**, *14*, 3090−3099.

(23) Ashok, A.; Kumar, A.; Ponraj, J.; Mansour, S. A.; Tarlochan, F. Single step synthesis of porous NiCoO2 for effective electrooxidation of glycerol in alkaline medium. *J. Electrochem. Soc.* **2018**, *165*, J3301−J3309.

(24) Kumar, A.; Wolf, E. E.; Mukasyan, A. S. Solution combustion synthesis of metal nanopowders: Copper and copper/nickel alloys. *AIChE J.* **2011**, *57*, 3473−3479.

(25) Kumar, A.; Wolf, E. E.; Mukasyan, A. S. Solution combustion synthesis of metal nanopowders: Nickel-Reaction pathways. *AIChE J.* **2011**, *57*, 2207−2214.

(26) Nazir, R.; Kumar, A.; Ali, S.; Saad, M. A. S.; Al-Marri, M. J. Galvanic Exchange as a Novel Method for Carbon Nitride Supported CoAg Catalyst Synthesis for Oxygen Reduction and Carbon Dioxide Conversion. *Catalysts* **2019**, *9*, 860.

(27) Ethiraj, A. S.; Kang, D. J. Synthesis and characterization of CuO nanowires by a simple wet chemical method. *Nanoscale Res. Lett.* **2012**, *7*, 70.

(28) Nazir, R.; Kumar, A.; Ali Saleh Saad, M.; Ali, S. Development of CuAg/Cu2O nanoparticles on carbon nitride surface for methanol oxidation and selective conversion of carbon dioxide into formate. *J. Colloid Interface Sci.* **2020**, *578*, 726−737.

(29) Yi, T.; Guo, C.; Zhao, S.; Zhan, K.; Gao, W.; Yang, L.; Du, G. The simultaneous preparation of nano cupric oxide (CuO) and phenol formaldehyde (PF) resin in one system: aimed to apply as wood adhesives. *Eur. J. Wood Wood Prod.* **2020**, *78*, 471.

(30) Xu, C.; Cheng, L.; Shen, P.; Liu, Y. Methanol and ethanol electrooxidation on Pt and Pd supported on carbon microspheres in alkaline media. *Electrochem. Commun.* **2007**, *9*, 997−1001.

(31) Hameed, R. M. A.; El-Khatib, K. M. Ni−P and Ni−Cu−P modified carbon catalysts for methanol electro-oxidation in KOH solution. *Int. J. Hydrog. Energy* **2010**, *35*, 2517−2529.

(32) Ojani, R.; Raoof, J.-B.; Ahmady-Khanghah, Y. Copper-poly (2-aminodiphenylamine) as a novel and low cost electrocatalyst for electrocatalytic oxidation of methanol in alkaline solution. *Electrochim. Acta* **2011**, *56*, 3380−3386.

(33) Venkatasubramanian, R.; He, J.; Johnson, M. W.; Stern, I.; Kim, D. H.; Pesika, N. S. Additive-mediated electrochemical synthesis of platelike copper crystals for methanol electrooxidation. *Langmuir* **2013**, *29*, 13135−13139.
(34) Periasamy, A. P.; Liu, J.; Lin, H.-M.; Chang, H.-T. Synthesis of copper nanowire decorated reduced graphene oxide for electro-oxidation of methanol. *J. Mater. Chem. A* **2013**, *1*, 5973−5981.
(35) Jing, L.; Lijun, L.; Yuting, Y.; Yanfang, G.; Jinrong, L. Fabrication of copper-ceria hybrid composite electrode for electro-catalytic oxidation of methanol. *J. Rare Earths* **2013**, *31*, 296−301.
(36) Zhang, R.; Li, Y.; Qi, J.; Gao, D. Ferromagnetism in ultrathin MoS 2 nanosheets: from amorphous to crystalline. *Nanoscale Res. Lett.* **2014**, *9*, 586.
(37) Xia, L.-P.; Guo, P.; Wang, Y.; Ding, S.-Q.; He, J.-B. Multi-laminated copper nanoparticles deposited on conductive substrates for electrocatalytic oxidation of methanol in alkaline electrolytes. *J. Power Sources* **2014**, *262*, 232−238.
(38) Das, A. K.; Layek, R. K.; Kim, N. H.; Jung, D.; Lee, J. H. Reduced graphene oxide (RGO)-supported NiCo 2 O 4 nano-particles: an electrocatalyst for methanol oxidation. *Nanoscale* **2014**, *6*, 10657−10665.
(39) Al-Sharif, M. S.; Arunachalam, P.; Abiti, T.; Amer, M. S.; Al-Shalwi, M.; Ghanem, M. A. Mesoporous cobalt phosphate electro-catalyst prepared using liquid crystal template for methanol oxidation reaction in alkaline solution. *Arabian J. Chem.* **2020**, *13*, 2873−2882.
(40) Arunachalam, P.; Shaddad, M. N.; Alamoudi, A. S.; Ghanem, M. A.; Al-Mayouf, A. M. Microwave-assisted synthesis of Co3 (PO4) 2 nanospheres for electrocatalytic oxidation of methanol in alkaline media. *Catalysts* **2017**, *7*, 119.
(41) Ehsani, A.; Jaleh, B.; Nasrollahzadeh, M. Electrochemical properties and electrocatalytic activity of conducting polymer/copper nanoparticles supported on reduced graphene oxide composite. *J. Power Sources* **2014**, *257*, 300−307.
(42) Ghouri, Z. K.; Barakat, N. A.; Kim, H. Y. Influence of copper content on the electrocatalytic activity toward methanol oxidation of Co χ Cu y alloy nanoparticles-decorated CNFs. *Sci. Rep.* **2015**, *5*, 16695.
(43) Cheng, J.; Yan, H.; Lu, Y.; Qiu, K.; Hou, X.; Xu, J.; Han, L.; Liu, X.; Kim, J.-K.; Luo, Y. Mesoporous CuCo 2 O 4 nanograsses as multi-functional electrodes for supercapacitors and electro-catalysts. *J. Mater. Chem. A* **2015**, *3*, 9769−9776.
(44) Pawar, S. M.; Kim, J.; Inamdar, A. I.; Woo, H.; Jo, Y.; Pawar, B. S.; Cho, S.; Kim, H.; Im, H. Multi-functional reactively-sputtered copper oxide electrodes for supercapacitor and electro-catalyst in direct methanol fuel cell applications. *Sci. Rep.* **2016**, *6*, 21310.
(45) Pawar, S. M.; Pawar, B. S.; Inamdar, A. I.; Kim, J.; Jo, Y.; Cho, S.; Mali, S. S.; Hong, C. K.; Kwak, J.; Kim, H.; Im, H. In-situ synthesis of Cu (OH) 2 and CuO nanowire electrocatalysts for methanol electro-oxidation. *Mater. Lett.* **2017**, *187*, 60−63.
(46) Lan, Y.; Ma, S.; Lu, J.; Kenis, P. J. Investigation of a Cu (core)/CuO (shell) catalyst for electrochemical reduction of CO2 in aqueous soultion. *Int. J. Electrochem. Sci.* **2014**, *9*, 7300−7308.
(47) Nazir, R.; Kumar, A.; Saleh Saad, M. A.; Ashok, A. Synthesis of hydroxide nanoparticles of Co/Cu on carbon nitride surface via galvanic exchange method for electrocatalytic CO2 reduction into formate. *Colloids Surf., A* **2020**, *598*, 124835.
(48) Zhu, X.; Gupta, K.; Bersani, M.; Darr, J. A.; Shearing, P. R.; Brett, D. J. L. Electrochemical reduction of carbon dioxide on copper-based nanocatalysts using the rotating ring-disc electrode. *Electrochim. Acta* **2018**, *283*, 1037−1044.
(49) Clark, E. L.; Hahn, C.; Jaramillo, T. F.; Bell, A. T. Electrochemical CO_2 reduction over compressively strained CuAg surface alloys with enhanced multi-carbon oxygenate selectivity. *J. Am. Chem. Soc.* **2017**, *139*, 15848−15857.
(50) Sun, Z.; Talreja, n.; Tao, H.; Texter, J.; Muhler, M.; Strunk, J.; Chen, J. Catalysis of Carbon Dioxide Photoreduction on Nanosheets: Fundamentals and Challenges. *Angew. Chem., Int. Ed.* **2018**, *57*, 7610−7627.

https://dx.doi.org/10.1021/acs.langmuir.0c02554
Langmuir 2020, 36, 12760−12771